Synoptic drivers of 400 years of summer temperature and precipitation variability on Mt. Olympus, Greece

Article *in* Climate Dynamics · September 2014

DOI: 10.1007/s00382-014-2313-3

CITATIONS
49

READS
659

5 authors, including:

Stefan Klesse
Swiss Federal Institute for Forest, Snow and Landscape Research WSL
52 PUBLICATIONS **2,242** CITATIONS
SEE PROFILE

Valerie Trouet
The University of Arizona
136 PUBLICATIONS **11,135** CITATIONS
SEE PROFILE

Clim Dyn
DOI 10.1007/s00382-014-2313-3

Synoptic drivers of 400 years of summer temperature and precipitation variability on Mt. Olympus, Greece

Stefan Klesse · Malin Ziehmer · Georgios Rousakis · Valerie Trouet · David Frank

Received: 3 June 2014 / Accepted: 25 August 2014

Abstract The Mediterranean region has been identified as a global warming hotspot, where future climate impacts are expected to have significant consequences on societal and ecosystem well-being. To put ongoing trends of summer climate into the context of past natural variability, we reconstructed climate from maximum latewood density (MXD) measurements of *Pinus heldreichii* (1521–2010) and latewood width (LWW) of *Pinus nigra* (1617–2010) on Mt. Olympus, Greece. Previous research in the northeastern Mediterranean has primarily focused on inter-annual variability, omitting any low-frequency trends. The present study utilizes methods capable of retaining climatically driven long-term behavior of tree growth. The LWW chronology corresponds closely to early summer moisture variability (May–July, r = 0.65, $p < 0.001$, 1950–2010), whereas the MXD-chronology relates mainly to late summer warmth (July–September, r = 0.64, $p < 0.001$; 1899–2010). The chronologies show opposing patterns of decadal variability over the twentieth century (r = −0.68, $p < 0.001$) and confirm the importance of the summer North Atlantic Oscillation (sNAO) for summer climate in the northeastern Mediterranean, with positive sNAO phases inducing cold anomalies and enhanced cloudiness and precipitation. The combined reconstructions document the late twentieth—early twenty-first century warming and drying trend, but indicate generally drier early summer and cooler late summer conditions in the period ~1700–1900 CE. Our findings suggest a potential decoupling between twentieth century atmospheric circulation patterns and pre-industrial climate variability. Furthermore, the range of natural climate variability stretches beyond summer moisture availability observed in recent decades and thus lends credibility to the significant drying trends projected for this region in current Earth System Model simulations.

Keywords Tree ring · Summer North Atlantic Oscillation · Northeastern Mediterranean · Maximum latewood density · Summer climate reconstruction · Latewood width

Electronic supplementary material The online version of this article (doi:10.1007/s00382-014-2313-3) contains supplementary material, which is available to authorized users.

S. Klesse (✉) · D. Frank
Swiss Federal Research Institute WSL, 8903 Birmensdorf, Switzerland
e-mail: stefan.klesse@wsl.ch

S. Klesse · M. Ziehmer · D. Frank
Oeschger Centre for Climate Change Research, 3012 Bern, Switzerland

M. Ziehmer
Physics Institute, University of Bern, 3012 Bern, Switzerland

G. Rousakis
Litohoro Forest Service, 602000 Litohoro, Greece

V. Trouet
Laboratory of Tree-Ring Research, University of Arizona, Tucson, AZ 85721, USA

1 Introduction

The Mediterranean Basin is a region where future climate impacts are expected to be severe and far-reaching (IPCC 2013; Giorgi and Lionello 2008). Warming trends and concomitant reductions in precipitation are expected to increase drought stress (Gao and Giorgi 2008) thereby affecting the intense agriculture activities (Schröter et al. 2005) and increasing fire risk across this region (Moriondo

Published online: 09 September 2014

et al. 2006). Projections of increasing summer heatwave frequency are most severe for low-altitude river basins and coastal regions, implying increasing health risks in many densely populated urban centers (Fischer and Schär 2010). Climate model comparisons show general consistency in warming and drying trends in the Mediterranean Basin, but with considerable uncertainties concerning absolute magnitude and spatial patterns of these changes (Planton et al. 2012).

General Circulation Models predict an overall drying of the Mediterranean region by the end of the twenty-first century of up to 20 % (IPCC 2013). However, analyses of instrumental measurements have demonstrated different climate modes and atmospheric drivers across the Mediterranean basin. In particular, the evolution of precipitation-related events during summer and autumn over the eastern Mediterranean regions generally differs from the western Mediterranean (Hertig et al. 2013). Moisture trends also differ by season. Depending on the scenarios used for downscaling approaches, summer precipitation predictions for the eastern Mediterranean range from a slight increase and a shortening of extreme dry spells (scenario A1B, Hertig et al. 2013) towards a severe drying (A2, Önol et al. 2014; Dubrovský et al. 2013). The winter period (October–May), however, when most of the annual precipitation occurs, is expected to exhibit negative precipitation anomalies independent of methods and scenarios (Hertig and Jacobeit 2008; Önol et al. 2014). These spatially and seasonally variable climatic trends will have various impacts on biophysical attributes. The overall drying trends for winter may negatively impact annual streamflow and agricultural activities (García-Ruiz et al. 2011), whereas the reduction of summer precipitation mainly results in a decline of forest productivity (Lindner et al. 2010).

Northeastern Mediterranean precipitation trends are most closely associated with storm-track changes that are controlled by large-scale circulation patterns, such as the North Atlantic Oscillation (NAO), the East Atlantic/Western Russia pattern (EA/WRUS), or the Scandinavian pattern (SCAND) (Quadrelli et al. 2001; Trigo et al. 2002; Dünkeloh and Jacobeit 2003; Xoplaki et al. 2004; Krichak and Alpert 2005). Summer air temperatures and precipitation in the Northeastern Mediterranean are modulated by blocking conditions and by an east–west geopotential height (GPH) dipole (Xoplaki et al. 2003a; Mariotti and Arkin 2007). This atmospheric circulation pattern during summer is part of the summer North Atlantic Oscillation (sNAO), which is defined as the first eigenvector of daily extratropical North Atlantic–European mean sea-level pressure during high summer (July–August, Folland et al. 2009). The sNAO has an influence on air temperature, meridional atmospheric circulation, and cloudiness over the northeastern Mediterranean by modulating the Anatolian Low (Chronis et al. 2011). Positive sNAO phases are associated with cold anomalies, enhanced cloudiness and precipitation in the Northeastern Mediterranean, and prominent teleconnections of the opposing conditions over the British Isles (Folland et al. 2009). This atmospheric circulation pattern not only influences climatic variability on seasonal to inter-annual timescales (Önol and Semazzi 2009; Xoplaki et al. 2004), but also on decadal to centennial timescales (Mariotti and Dell'Aquila 2012; Luterbacher et al. 2010; Trouet et al. 2012).

In light of the inter-annual to multi-decadal dynamics, long climatic records are needed to quantify and understand trends in natural climate variability. Furthermore, placing the sizable trends in temperature, precipitation and drought stress projected for the next century in the Mediterranean basin requires long-term climate records. The paucity of instrumental records in the northeastern Mediterranean prior to 1950 hamper such assessments. Thus, proxy-based reconstructions (Luterbacher et al. 2002; Nicault et al. 2008; Pauling et al. 2006) contribute to our understanding of long-term climate variation in this region.

In terms of high-resolution proxy archives from the northeastern Mediterranean, tree line forests (*Pinus heldreichii,* PIHE in particular) have shown a strong dendroclimatological potential (Trouet et al. 2012; Seim et al. 2012; Trouet, in press) for reconstructing summer temperature by means of maximum latewood density (MXD) over the last millennium. Other studies have shown the potential of long-living Mediterranean tree species to reconstruct precipitation during the growing season, including *Quercus sp.* (Griggs et al. 2007*)* and *Juniperus excelsa* (Touchan et al. 2003). Tree-ring chronologies from the wide-spread and drought sensitive species black pine (*Pinus nigra,* PINI) have also been used in regional precipitation reconstructions (e.g. Akkemik and Aras 2005; Köse et al. 2011; Poljanšek et al. 2012; Levanic et al. 2013). These reconstructions, however, have primarily focused on high frequency (interannual) climate variability. The detrending techniques (often individual curve fits) applied, subsequent autoregressive modelling, and sample sizes of ~20 samples per site have left potential longer-term trends in past climate broadly unknown. Furthermore, detailed assessment of long-term climate variation is hampered by prior individual works solely reconstructing either temperature or precipitation. To simultaneously understand temperature and hydroclimatic variability, the climate history still must be pieced together from the few sparse and spatially disparate reconstructions.

In this study we present robust reconstructions of climatic variability in the northeastern Mediterranean basin by developing and analyzing an extensive tree-ring collection from Mt. Olympus, Greece. The significant ecological gradient on the Mt. Olympus massif causes temperature

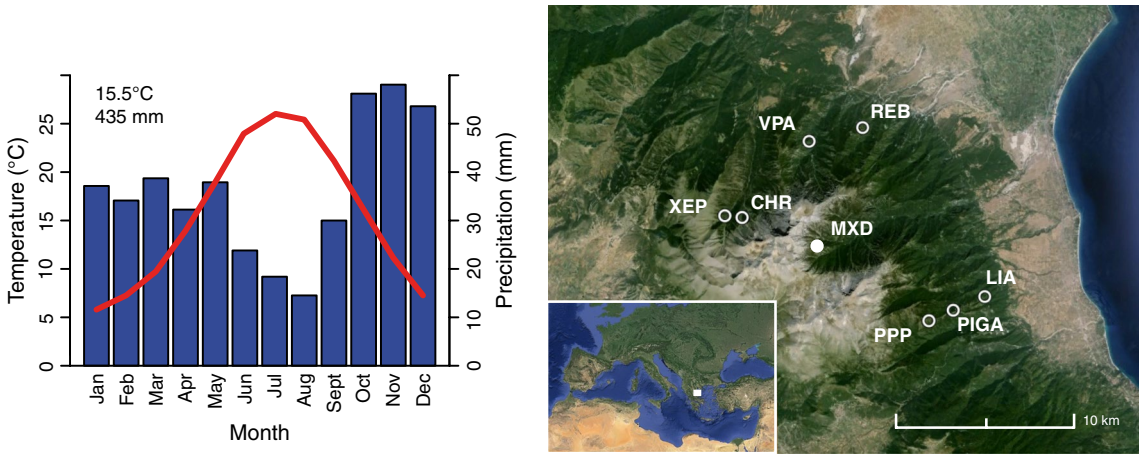

Fig. 1 Climate diagram of the nearest meteorological station Larissa (74 m asl) and map of Mt. Olympus (Greece) with sampled PINI LWW (*open circles*) and PIHE MXD (*filled circle*) sites

limitations on tree growth towards the upper-treeline and moisture stress along the lower mountain flanks. Based on more than 500 tree cores from 9 sites, we present new summer climate reconstructions for temperature and precipitation over the past 400 years derived from MXD (PIHE) and latewood width (LWW) chronologies (PINI). We focus on long-term trends and variability and their association with atmospheric circulation patterns.

2 Materials and methods

2.1 Study area

Mt. Olympus, situated in northern Greece, is part of the NNW–SSE oriented dinaric-hellenic mountain arc (Fig. 1). Only 20 km from the coastline, the massif peaks at 2,917 m (Mitikas). A typical Mediterranean dry season occurs from May to September with highest mean temperatures in July and August around 25 °C at the foot of the mountain in Larissa (50 km south, 74 m asl). The joint limestone bedrock rapidly absorbs rainfall and snowmelt so that surface runoff is scarce above 1,200 m asl. PINI often forms pure stands on dry and rocky slopes between 800 and 1,700 m asl, whereas beech (*Fagus sylvatica*) forests dominate the valley bottoms and ravines with moister conditions. At 1,600 to 2,000 m asl, PINI is gradually replaced by PIHE, which forms the upper treeline near 2,300 m asl (Strid 1980).

2.2 Tree ring data and analysis

2.2.1 Development of PINI LWW chronology

Our seven PINI sampling sites span the lower to upper elevation range (850–1,700 m asl) of the species in this region and are distributed around the Mt. Olympus massif to capture different slope exposures and luff-lee conditions. We collected at least two cores per tree from 33 to 48 trees per site (Fig. 1; Table 1). The cores were mounted, sanded, and cross-dated using standard dendrochronological techniques (Stokes and Smiley 1968). During sample preparation and cross-dating, we noted strong and coherent variability in the LWW. By using only LWW, Meko and Baisan (2001) and Griffin et al. (2011) were able to enhance the monsoonal precipitation signal (July–August) in tree rings of the southwest United States and thus extract much cleaner and temporally more specific climate information than by analyzing total TRW. Accordingly, we measured earlywood (EWW), and LWW separately to the nearest 0.01 mm using TSAP-Win software (Rinn 2003) and quality-checked the cross-dating using the program COFECHA (Holmes 1983). Signal-free Regional Curve Standardization (RCS) was applied to all individual LWW series to enhance retention of possible low frequency signals while retaining high frequency variability (Melvin and Briffa 2008). In RCS, the individual series are first aligned by cambial age to obtain a regional growth curve (RC), by which they are subsequently divided (Briffa et al. 1992). Signal-free detrending removes possible distortion of the external forcing signal in chronologies by iteratively dividing ring width measurements by the chronology index (Melvin and Briffa 2008). Each site chronology was detrended with its own RC smoothed with an age-dependent spline (Melvin et al. 2007), using pith off-set estimates to improve the accuracy of the expected growth curve (Briffa and Melvin 2011). Site-level detrending was necessary because of differences in absolute growth level between sites and changing site replication over time (Fig. 2a, Klesse and Frank 2013). The site CHR differed notably in its site condition, stand composition, and low frequency behavior from the other six

Table 1 Raw chronology statistics

Site	Species	Ring parameter	Elevation (m asl)	Latitude	Longitude	Chronology[a]	MSL	n Trees	n samples	Rbar	MS
LIA	PINI	LWW	850	40.050041	22.497186	1853–2010	96.3	45	87	0.57	.471
VPA	PINI	LWW	1,050	40.135815°	22.366780°	1794–2010	143	33	66	0.627	.486
REB	PINI	LWW	1,100	40.143893°	22.406005°	1848–2010	133.8	47	92	0.679	.525
PIGA	PINI	LWW	1,300	40.042421°	22.474153°	1607–2010	255.8	41	73	0.563	.474
XEP	PINI	LWW	1,500	40.093058°	22.308132°	1604–2010	267.2	31	78	0.519	.352
PPP	PINI	LWW	1,600	40.036644°	22.456621°	1617–2010	242	40	79	0.632	.444
CHR	PINI	LWW	1,700	40.092192°	22.321162°	1794–2010	167.7	42	81	0.553	.331
combined	PIHE	MXD	2,200	40.09°	22.37°	1521–2010	312	50	96	0.312	.044
Old (1981)	PIHE	MXD	2,200			1698–1981	201	15	29	0.327	.043
New (2010)	PIHE	MXD	2,200			1521–2010	361	35	67	0.310	.045

PINI Pinus nigra, *PIHE* Pinus heldreichii, *LWW* latewood width, *MXD* maximum latewood density, *MSL* mean segment length, *Rbar* series intercorrelation, *MS* mean sensitivity

[a] EPS > 0.85

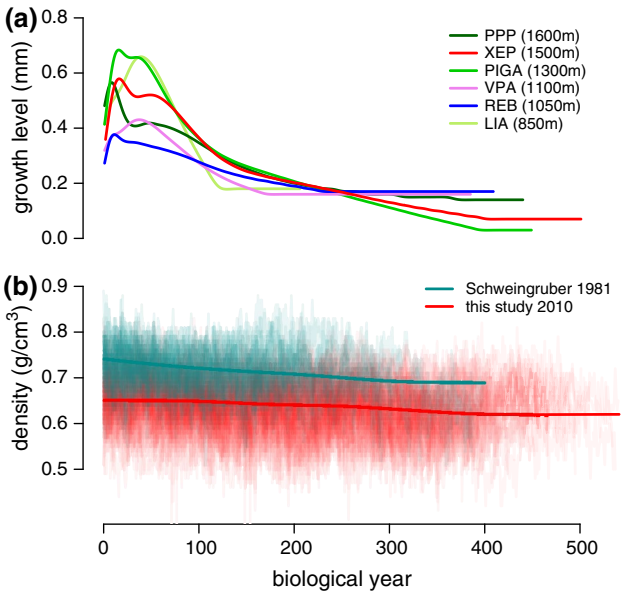

Fig. 2 **a** Individual LWW growth curves, smoothed with an age-dependent spline and **b** the regional curves of the two separate MXD datasets (300-year spline). The *flat line* at the end of the *curves* indicates truncation of the fitting due to a sample replication <5

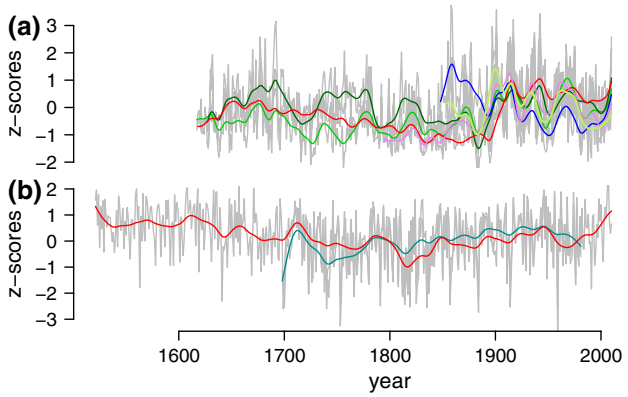

Fig. 3 Detrended PINI LWW chronologies (**a**) and PIHE MXD chronologies (**b**). To improve visibility, the single chronologies were smoothed with a 30-year spline

sites and it was excluded from the reconstruction (for further information the reader is referred to Klesse and Frank 2013). The remaining six chronologies (Fig. 3a) were scaled to match their mean and variance over the common period (1853–2010) and averaged with a bi-weight robust mean (Cook and Kairiukstis 1990) after variance stabilization due to changing site replication over time (Frank et al. 2006). Chronology reliability was assessed using the expressed population signal (EPS), which is calculated from between-tree correlations (rbar) and sample replication. A threshold of 0.85 is often (albeit arbitrarily) cited as adequate to ensure the robustness of a chronology (Wigley et al. 1984). The resulting regional LWW chronology is considered reliable back to 1617, when three sites have an EPS higher than 0.85.

2.2.2 *Development of PIHE MXD chronology*

The PIHE samples were collected in the central part of Mt. Olympus close to tree line at around 2,200 m asl (Table 1) in 2010 to update, extend, and enhance an existing chronology collected by Schweingruber in 1981. The cores were prepared for MXD measurements after Schweingruber (1989). The prepared samples were processed using a WALESCH 2003 X-ray densitometer with a resolution of 0.01 mm and brightness variations transferred into g/cm^3 using a calibration wedge (Eschbach et al. 1995; Lenz et al. 1976). After cross-dating as described above, the MXD-series were detrended using signal-free RCS with

a 300-year spline smoothing. Pith-offset estimates (POE) were not available for the Schweingruber dataset. However, the slope of the RCs of the age aligned MXD measurements was quite shallow (Fig. 2b) and a lack of POE would not alter the RC dramatically, so for consistency we did not use pith offset data for the entire MXD dataset. The absolute density levels of the two datasets were offset from each other (Fig. 2b) likely due to a change in the X-Ray densitometry equipment and laboratory procedures between the early 1980s and present (different X-Ray films and calibration wedges, Esper et al. 2014) and possibly because of local site conditions. Thus for RCS, separate detrending of these two datasets was necessary (see also Grudd 2008). The two MXD_{RCS}-chronologies are strongly correlated ($r = 0.83$; $p < 0.01$). After standardization, the two chronologies were combined by scaling over their common period (EPS > 0.85, 1698–1981), and averaged as described with the *PINI* chronologies, resulting in a robust MXD chronology (EPS > 0.85) back to 1521.

2.3 Climate data

To assess the climate signal in the tree-ring data, its temporal stability, spatial signatures, and to define the most meaningful reconstruction target, we considered a wide variety of instrumental station records, gridded products, re-analyses, and previous reconstructions. In so doing, we attempted to balance properties of the instrumental datasets such as record length, data quality, and proximity to the tree-ring sites. The nearest meteorological station with records of relevant length is located in Larissa (74 m asl), approximately 50 km south of the massif, with temperature observations starting in 1899 and precipitation in 1951. The Larissa climate station is situated in flat terrain and southwest of the coastal ridgeline. Given its long length, and proximity to the tree sites, the Larissa instrumental temperature record (1899–2010) was used as a target for *PIHE*-based temperature analysis and reconstruction. However, the amount and occurrence of precipitation on Mt. Olympus varies with the position around the massif. Thus, the Larissa precipitation record may not be representative of the east-facing slopes of the mountainous study area, where summer precipitation is closely related to thunderstorms. Similar considerations and limitations apply for the other nearby stations, Thessaloniki (70 km NE), and Kozani (50 km NW), with precipitation records since 1931 and 1955. For this reason we used the gridded (0.25 × 0.25° resolution, 1950–2010) E-OBS dataset (Klein Tank et al. 2002; Haylock et al. 2008) to calculate climate–growth correlations between the chronologies and precipitation and temperature, and as the precipitation reconstruction target dataset. We preferred this relatively short dataset to the often cited CRU dataset (Mitchell and Jones 2005) to ensure more precise spatial coverage of the tree-ring sites and because the span of the E-OBS dataset corresponds closely to the span of the proximal meteorological records. Prior to 1950, the nearest long precipitation datasets include Athens and Patrai located 230 and 330 km south of Mt. Olympus. The impact of increasing station sparseness can be observed in the spatial correlation fingerprint between the Mt. Olympus CRU grid cell time series and the surrounding grid cells. Post 1950, high correlations ($r > 0.50$) are restricted to northeastern Greece, Macedonia, and southeast Bulgaria (Fig. S1), whereas prior to 1950 high correlation values cover Greece and the entire Balkans until 44°N. This is indicative of more remote (and less representative) stations become increasingly weighted in the CRU gridding approach when the proximal (e.g., within 100 km) stations are no longer available. These tests further support the preferential use of the E-OBS dataset.

Climate–growth responses were assessed based on Pearson correlation coefficients between the tree-ring data and monthly gridded climate data (E-OBS 7.0, 1950–2010) for the gridpoint closest to the study site (40.13°N, 22.13°E). Monthly values were further averaged to seasonal windows thereby integrating the most meaningful months of wood formation. To identify spatial signatures in the reconstructions over as long of a time-span as possible, we performed additional analyses with the long Larissa instrumental temperature record (1899–2010), the CRU temperature dataset (CRU 3.21, 1901–2010) and seasonal 500 mb GPH fields (Twentieth Century Reanalysis, 1901–2010; Compo et al. 2011). For the pre-instrumental period, we used seasonal historical gridded reconstructions of air temperature (Luterbacher et al. 2004), precipitation (Pauling et al. 2006), and 500mb GPH (Luterbacher et al. 2002). Spatial correlation and composite maps were generated using the KNMI explorer (http://climexp.knmi.nl; van Oldenborgh and Burgers 2005, Trouet and Van Oldenborgh 2013). We performed a Wilcoxon test to calculate the statistical significance of monthly 500mb GPH anomalies of the twentieth century over the Balkans and British Isles in years when the PIHE and PINI reconstructions both show positive/negative values or have opposing signs.

2.4 Reconstruction

The dimensionless tree-ring indices were calibrated to temperature and precipitation by scaling (i.e., matching the mean and standard deviation of the instrumental target over the calibration period; Esper et al. 2005). The long Larissa instrumental temperature record (1899–2010) as well as the E-OBS gridded temperature data (1950–2010) were used for July–September temperature calibration/verification trials. The LWW chronology was calibrated to the E-OBS May–July precipitation grid-cell data (40.13°N, 22.13°E)

expressed as anomalies from the 1950–2010 period. To test the reconstruction model, the Coefficient of Efficiency (CE) and Reduction of Error (RE) statistics (Cook et al. 1994; Frank and Esper 2005) were used to assess the skill of the reconstructions over two sub-periods (1950–1980 and 1981–2010 for the E-OBS data; 1899–1954 and 1955–2010 for Larissa temperature).

3 Results

3.1 Climate–growth relationships

The strong coherence among the individual LWW chronologies (Fig. 2a) suggests a common response to environmental conditions. Correlations among sites are stable in time and generally high, with inter-series correlation of the LWW chronologies ranging from r = 0.35 (LIA-XEP, altitudinal difference 650m, horizontal distance 16.5 km) to r = 0.80 (PIGA-PPP, 300 m, 1.5 km) over the 1853–2010 common period. As expected from the common growth patterns, all six sites show a similar climate response pattern (not shown, see Klesse 2012) and this justified averaging the six RCS chronologies into a regional chronology for further analyses without risking a change in climate response over time due to changing site replication. The main climatic driver of PINI growth is moisture availability during the summer months (Fig. 4a). Only weak correlations were found with climatic conditions in the previous year or spring preceding the growing season. Correlations were strongest with MJJ precipitation ($r_{EOBS} = 0.65$, $p < 0.001$), and June–July temperature ($r_{EOBS} = -0.51$, $p < 0.001$).

Correlations between the MXD series and E-OBS temperatures were positive and greater than r = 0.20 for the months April through September, with highest values in July and August (Fig. 4b). Temperatures averaged for these 2 months yielded correlations of r = 0.61 ($p < 0.001$), which was stronger than the negative correlations obtained with precipitation sums for these same 2 months ($r_{EOBS} = -0.46$, $r_{Larissa=} = -0.42$, Fig. 5b). Also the averaged July–September temperature response assessed with the E-OBS dataset was comparably strong (r = 0.57). Exploration of climate response over the longer Larissa temperature record (1899–2010) revealed the strongest, most consistent, and highly stable climate response with July–September (JAS) temperatures (e.g., r = 0.67, r = 0.63, and r = 0.64 for the early (1899–1949), late (1950–2010), and full periods, respectively).

3.2 Precipitation reconstruction

The climate response of the LWW dataset provided the opportunity to develop a summer precipitation reconstruction. Accordingly, we performed formal calibration/verification exercises (Table 2). For May–July precipitation, 37–42 % of the variance was explained in the verification procedure, indicating good reconstruction skill and a stable strength of the climate signal in the tree-ring record. This stability and the ability to capture lower frequency trends was confirmed by RE and CE statistics with positive values for both statistics during the early and late verification periods. Note that these statistics are provided for calibrations performed by scaling; corresponding statistics for regression approaches (for which the RE and CE statistics were developed) are even higher. A final MJJ precipitation reconstruction spanning the period 1617–2010 was performed by calibration over the full 1950–2010 period.

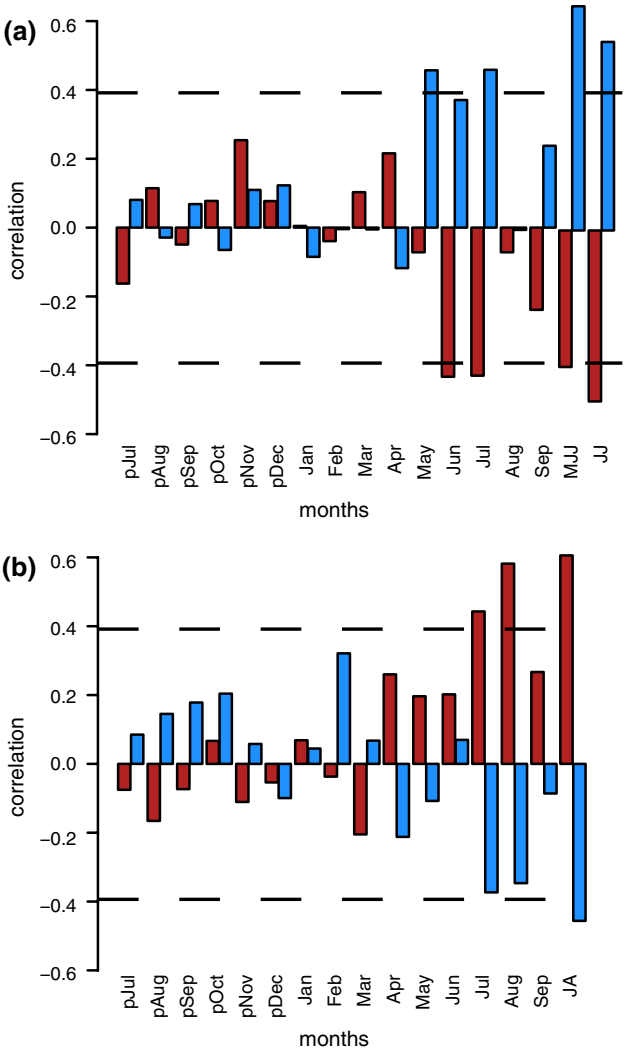

Fig. 4 Response of the LWW chronology (**a**) and the MXD chronology (**b**) to precipitation (*blue*) and temperature (*red*) over the period 1950–2010 with the E-OBS gridded dataset (40.13°N, 22.13°E). *Dashed lines* represent the significance level $p < 0.001$

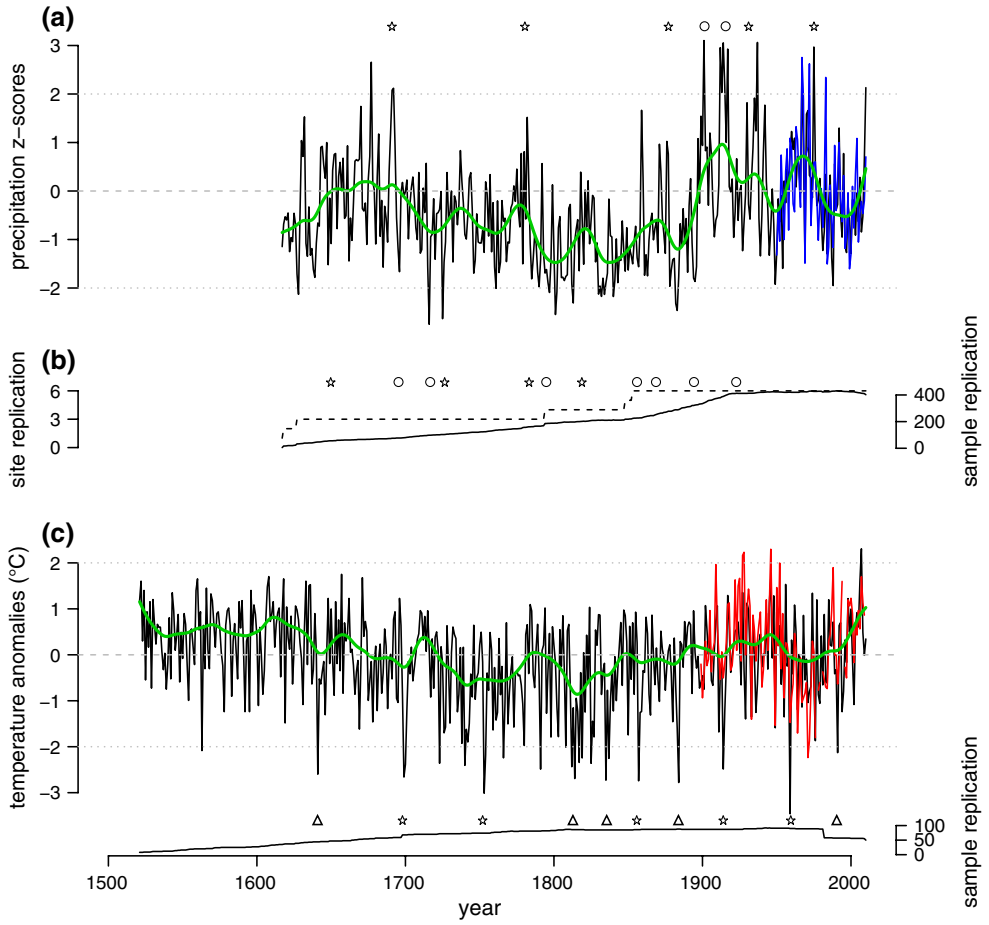

Fig. 5 Actual and reconstructed May–July precipitation (**a**) and July–September temperature anomalies (**b**) with a 30-year spline smoothing (*green*) and sample and site replication over time. *Triangles* mark major volcanic eruptions, *asterisks* (*circles*) represent pointer years (periods with two or more consecutive extreme years) also mentioned in other climate reconstruction literature of the Eastern Mediterranean

Table 2 Calibration and verification statistics of both temperature (MXD) and precipitation (LWW) reconstructions

	E-OBS		Larissa	
	Early calibration period (1950–1980)	Late calibration period (1981–2010)	Early calibration period (1899–1954)	Late calibration period (1955–2010)
MXD				
R2	0.403	0.281	0.460	0.388
RE	0.292	0.339	0.183 (0.339)[a]	0.367 (0.382)[a]
CE	0.148	0.166	−0.063 (0.140)[a]	0.150 (0.140)[a]
LWW				
R2	0.343	0.413		
RE	0.368	0.313		
CE	0.172	0.165		

RE reduction of error, *CE* coefficient of efficiency

[a] Values in brackets show results after regression instead of scaling

The precipitation reconstruction shows a continuous decline over ca. 200 years (1700–1896) before an abrupt rise around the turn of the twentieth century (Fig. 5a). The beginning of the twentieth century (1901–1917) appears to have been the wettest early summer period in the past 400 years. The late twentieth century drying trend (1975–2000), known from

instrumental data, is also well captured by the tree-ring data but is reversed in the twenty-first century. The reconstruction suggests that the majority of the twentieth Century (~1900–1975) was the wettest period on record and that recent moisture deficits are well within the range of natural variability experienced over the past 400 years.

3.3 Temperature reconstruction

Similarly, the climate response of the MXD record demonstrates the potential to develop a July–September temperature reconstruction. A skillful and stable calibration model was indicated by positive RE and CE statistics using the JAS E-OBS temperature data (1950–2010) as a target (Table 2). The final test with the long Larissa temperature data (1899–2010) revealed a positive RE and a slightly negative (−0.063) CE statistic suggesting some discrepancies on centennial time-scales. Attribution of these low-frequency discrepancies remains challenging as previous research has indicated significant uncertainties with the trends of long instrumental records (Wilson et al. 2005; Frank et al. 2007; Böhm et al. 2010; Thompson et al. 2008) in addition to those found in proxy data. Furthermore, in the case of the Larissa- MXD calibration, the agreement remains good with overall positive calibration statistics (RE: 0.339, CE: 0.140) when using linear regression rather than scaling. Considering the uncertainties in both the tree-ring and instrumental data and the lower variance of the reconstruction in comparison to the instrumental data when using regression (Esper et al. 2005), and the desire to maximize the calibration window, the final reconstruction was developed by scaling to the Larissa temperatures over the full 1899–2010 period.

The Mt. Olympus temperature reconstruction (1521–2010) displays overall decreasing late summer temperatures from the seventeenth century to the early nineteenth century (Fig. 5b). The coldest decade in our record occurred from 1811 to 1820 and only 2 years of the eighteenth and nineteenth century rank among the 50 warmest, thus showing pronounced cool summer temperatures during that time. Over the most recent century, the temperature reconstruction closely tracks well interannual to multi-decadal variations of the Larissa JAS-temperature record, including the ongoing warming trend from 1975 to the present (Fig. 5b). Summer temperatures of the last decade are at the upper end of reconstructed values, the summer of 2007 is the warmest over the past 490 years, but the above average temperatures of the sixteenth and early seventeenth century were likely more persistent.

3.4 Spatial dynamics and teleconnections

Spatial correlation analysis between our JAS temperature reconstruction and JAS instrumental temperature (Fig. 6a, b) and JAS 500mb GPH (Fig. 6c) reveals a strong dipole pattern across Europe over the modern instrumental period. The MXD-based temperature reconstruction is highly representative of conditions in the northeastern Mediterranean and negatively correlated with conditions over the British Isles. This pattern has broadly the same extent and strength in the early (1901–1949) as in the late instrumental period (1950–2010) and is stable also over the pre-instrumental period (1659–1900, Fig. 6d). A strong correlation was observed between the Mt. Olympus MXD chronology and other PIHE MXD records from the eastern Mediterranean. Correlation values in the inter-annual to multi-decadal domain (i.e., data detrended with a 100-year spline) are: $r = 0.78$ (Vihren, Bulgaria, common period 1790–1981, collected by Schweingruber 1981, NCDC 2011, $p < 0.001$); $r = 0.67$ (Mt. Pollino, Italy, 1660–1980, collected by Schweingruber 1981, NCDC 2011, $p < 0.001$); and 0.63 (Albania, 1521–1895, unpublished, $p < 0.001$). The positive correlation in the northeastern Mediterranean and negative correlation centered over the British Isles are consistent with the atmospheric circulation pattern known as the summer North Atlantic Oscillation (sNAO; Folland et al. 2009). Accordingly, the correlations between our temperature reconstruction and NCEP-sNAO index (JAS, 1948–2010) and UCAR-sNAO index (JAS, 1899–2010) are $r = -0.535$, $p < 0.001$ and $r = -0.505$, $p < 0.001$ respectively. Our reconstruction also shows persistent agreement with the sNAO reconstruction developed by Linderholm et al. (2009, 1521–1995, $r = -0.33$, $p < 0.001$) based entirely on tree-ring data from Scotland and Scandinavia.

The spatial signatures of the LWW-based precipitation reconstruction are similar to those of the temperature reconstruction, but are weaker in strength (Fig. 7). Our reconstruction of MJJ precipitation is significantly positively correlated with MJJ precipitation patterns in the Balkans and to a weak extent negatively correlated with precipitation in NW France. The spatial correlation to MJJ temperature is strongly significant in the Balkans, southern Italy, and parts of northern Africa and the Levant (Fig. 7b). We also find a regional coherence with other precipitation sensitive records prior to the instrumental period. For example, the high-frequency (2–15 years bandpass filtered) Mt. Olympus precipitation reconstruction correlates strongly with the PINI TRW chronologies developed by Kuniholm in northern Greece at Zagradenye ($r = 0.59$, 1751–2003, distance = 230 km NE, $p < 0.001$) and Scotida ($r = 0.62$, 1706–1979, 160 km W, $p < 0.001$), indicating a representative and stable summer moisture signal for northern Greece recorded by PINI on Mt. Olympus.

3.5 Temperature and precipitation co-variability

Our new reconstructions from Mt. Olympus offer the opportunity to assess the co-variation between

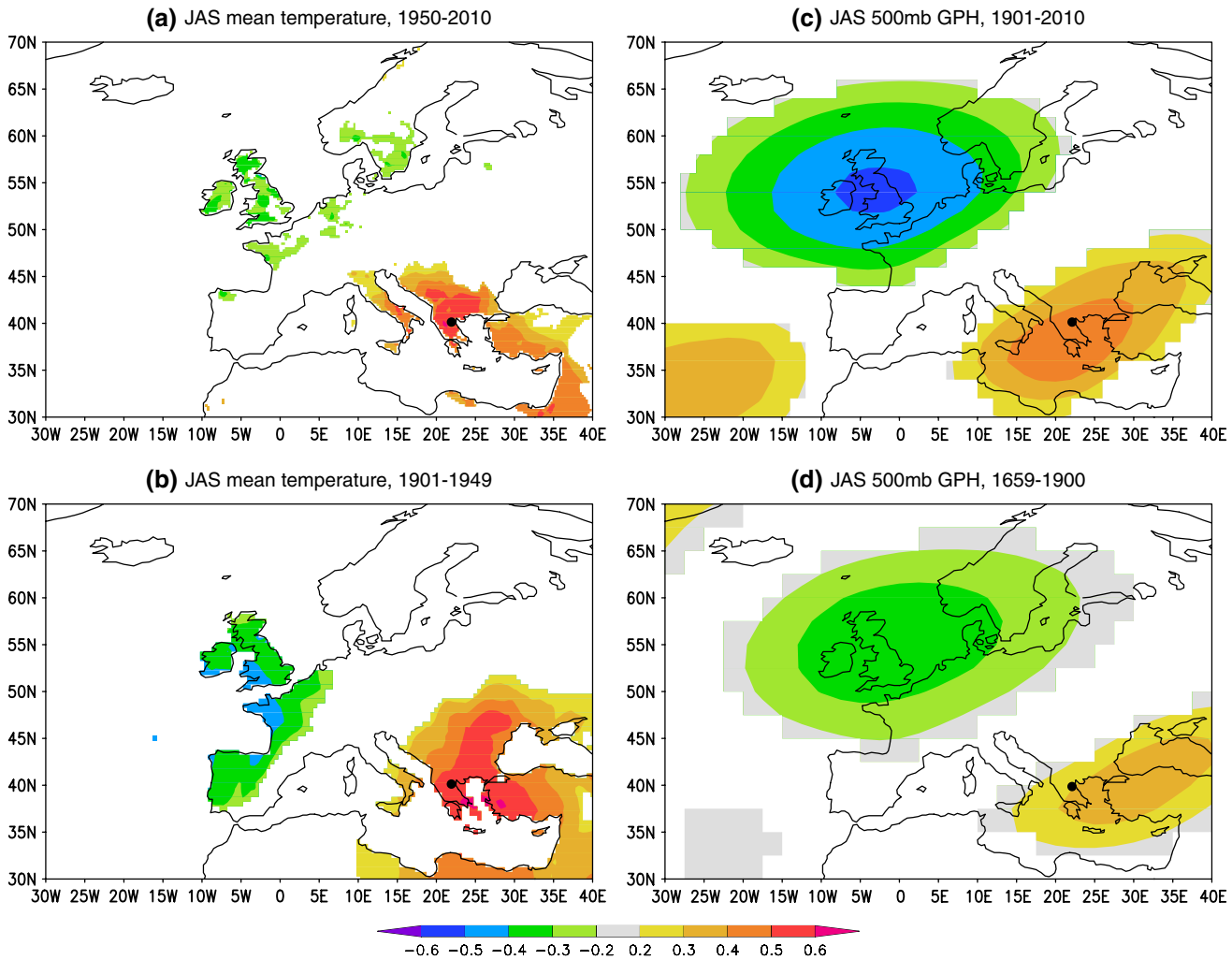

Fig. 6 Spatial correlation maps between the MXD chronology and **a** July–September (JAS) mean temperature (E-OBS, 1950–2010), **b** JAS mean temperature (CRU, 1901–1949), **c** JAS 500mb GPH (20C reanalysis) and **d** JAS 500mb GPH reconstruction (Luterbacher et al. 2002). The study site is indicated by a *black dot* on the maps

temperature and precipitation over the past 400 years. These reconstructions show a weak negative inter-correlation in their high-frequency domain (2–15 years bandpass-filtered) throughout their common period 1617–2010 ($r = -0.13$, $p < 0.05$, $r_{1950–2010} = -0.21$, $p = 0.1188$). Their medium-frequency variability (15–100 years) generally also correlates negatively over the full period ($r = -0.25$, $p < 0.001$). Running correlations with a 51-year window-length oscillate between +0.2 and −0.4 between 1617 and 1890. Although care must be taken when assessing the significance of low-frequency variability due to reduced degrees of freedom, the negative relationship is notably strong during the twentieth century ($r = -0.67$, $p < 0.001$). Similar relationships are observed in the meteorological data from 1950 to 2010, with the correlation between MJJ precipitation and JAS temperatures weaker in the high frequencies ($r = -0.26$, $p < 0.05$) than in the medium frequencies ($r = -0.58$, $p < 0.001$). These results indicate that cooler decades in the twentieth century have been accompanied by generally wetter conditions, while the year-to-year anti-correlation has been fairly weak. However, our two reconstructions suggest that this strong decadal co-variability has not been the case in the nineteenth century. From 1801 to 1850 the correlation between the mid-frequency filtered series is only $r = -0.29$ ($p < 0.05$) and turns even slightly positive from 1851 to 1900 ($r = +0.13$, $p = 0.38$). The nineteenth century is furthermore characterized by overall drier early summer conditions and generally cooler late summer temperatures. The different temporal response of the two reconstructions to summer climate offers the possibility to study the annual course of the atmospheric circulation patterns over Europe (e.g. 500mb GPH).

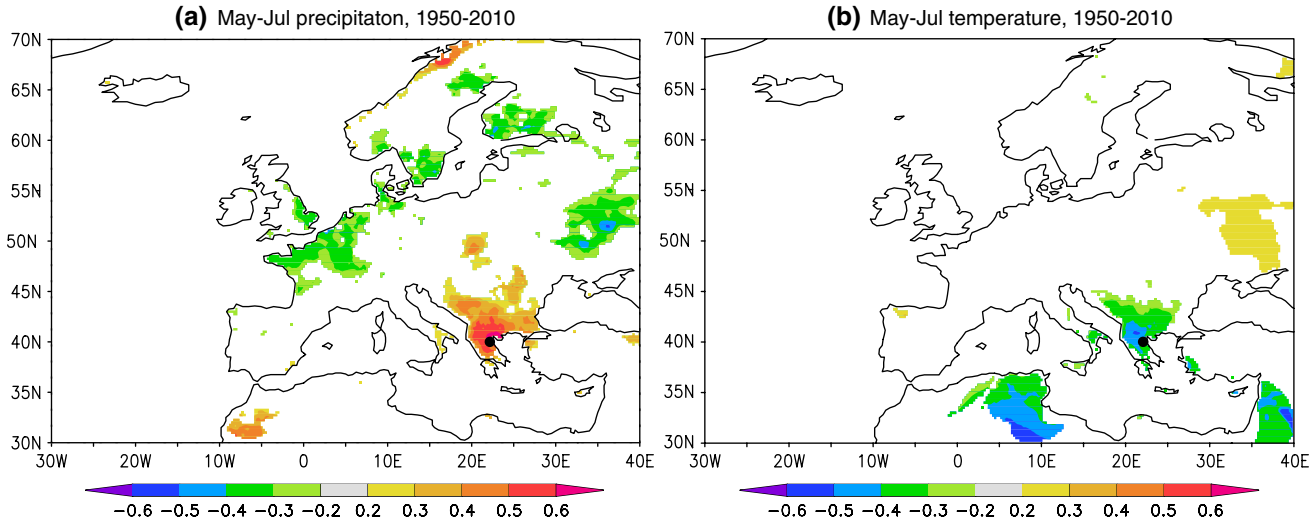

Fig. 7 Spatial correlation maps between the LWW chronology and **a** May–July precipitation and **b** May–July temperatures (both E-OBS). The study site is indicated by a *black dot* on the maps

During the 1901–2010 period (20C Reanalysis) cool and moist summer conditions (i.e. where the temperature reconstruction has values lower than the 1950–2010 average and the precipitation reconstruction higher values) have occurred 27 times (25 %). In these years there is a significant negative 500mb GPH deviation ($p < 0.05$) from June through September over the Balkans (37–47°N, 18–28°E, Fig. 8) and the sNAO-like dipole pattern is very pronounced from June through September (upper right panel in Fig. 9). Similarly, in warm and dry years (37 %), the positive anomaly pattern is persistent over the whole summer (Fig. 9). During the twentieth century dry and cool conditions have occurred only 16 times (15 %). In these years, the 500 mb GPH field follows a distinct course from negative anomalies in June to a ridge in August over the British Isles (50–60°N, -10–10°E, Fig. 8) and an opposing but weaker pattern over the Central to western Mediterranean in June and northeastern Mediterranean in August (lower left panels in Fig. 9). Warm and wet years (24 %) are characterized by a shift from a positive 500mb GPH anomaly in June to strong negative anomalies in late summer (especially August) over the British Isles (Fig. 8) and vice versa over the Balkans (lower right panels in Fig. 9). The dominance of dry (early) summer conditions and rather cool (late) summer conditions during the eighteenth and nineteenth century (44 and 47 %, respectively) suggests that drivers of atmospheric circulation over Europe during summer have changed in the last 110 years. This would be consistent with a stable center of action over the British Isles with lower 500 mb GPH in early summer and higher GPH during late summer, while the anomalies over the Mediterranean are of opposite sign. Circulation patterns in moist and cool summers as well as moist and warm summers of the twentieth century seem to have played a minor role over the previous two centuries (22 and 13 %, respectively).

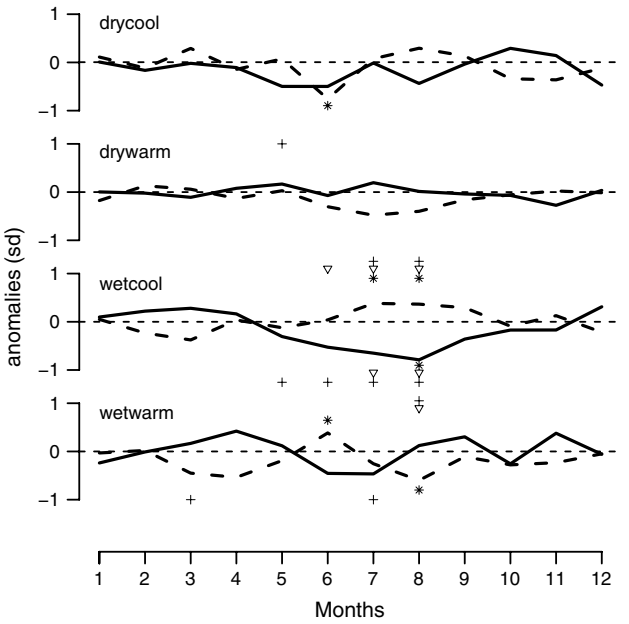

Fig. 8 Annual courses of composite 500 hPa normalized geopotential height anomalies over the British Isles (50–60°N, -10–10°E; *dashed line*) and the Balkans (37–47°N, 18–28°E; *full line*) between 1901 and 2010 (20C Reanalysis) when the LWW chronology <0 and the MXD chronology <0 (drycool), LWW <0 and MXD >= 0 (drywarm), LWW >= 0 and MXD < 0 (wetcool), and LWW >= and MXD >= 0 (wetwarm). *Asterisks* (*triangles, crosses*) show significant ($p < 0.05$) anomalies of single months (2-month averages, 3-month averages). *Symbols* are on *top* of the first month of the averaged period

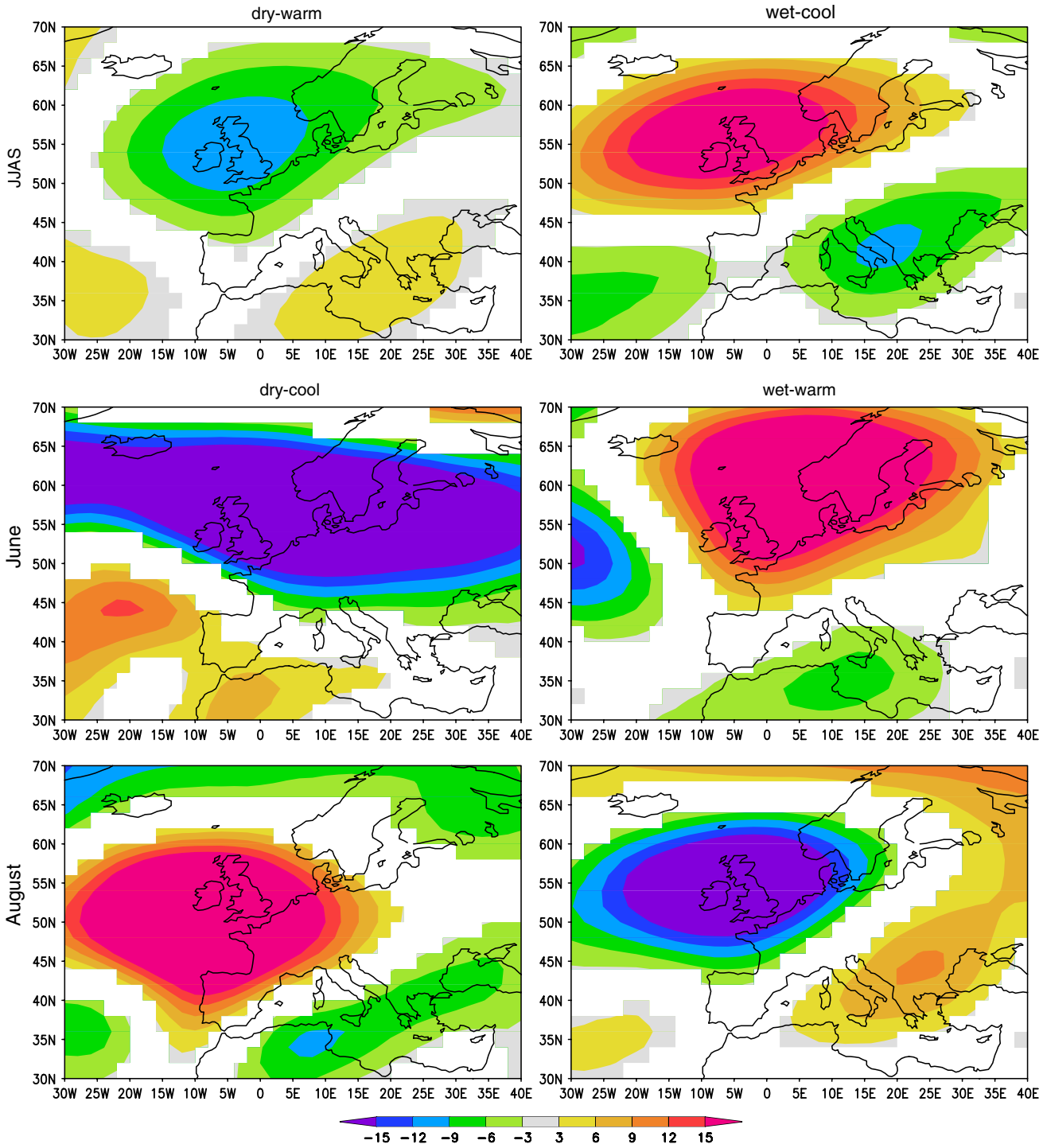

Fig. 9 Composite 500mb geopotential height anomaly maps (1901–2010, 20C Reanalysis, anomalies of the 1950–2010 period) for dry and warm (*top left*), wet and cool (*top right*), dry and cool (*bottom left*) and wet and warm summers (*bottom right*). The *top panels* show the persistence of the 500mb GPH anomalies from June to September, while the *lower panels* signify the sign change between the British Isles and the Mediterranean between early summer (June) and late summer (August). The specific years are defined as in the text and Fig. 8. Units of anomalies are tens of meters

4 Discussion

4.1 Inter-annual to centennial climate variability

We provided new proxy reconstructions for the northeastern Mediterranean allowing a joint assessment of summer temperature and precipitation variability since 1617 AD and associated dynamical drivers. While MXD chronologies have previously primarily been developed for the high latitude boreal zone, our investigation on PIHE trees from Mt. Olympus strongly supports the utility of this tree-ring parameter in lower latitude regions (Briffa et al. 1988; Büntgen et al. 2008, Trouet et al. 2012, Trouet, in press). The coldest decade in our temperature reconstruction occurred from 1811 to 1820 (−1.22 °C below the 1950–2010 average), which is in line with extremely cool summers reported throughout central Europe by long instrumental records (Böhm et al. 2010), tree-ring reconstructions (Büntgen et al. 2006, Frank and Esper 2005; Trachsel et al. 2012; Popa and Bouriaud 2014), and inferred from rapid glacier advances in the Alps (Zumbühl et al. 2008). This decade includes the year 1816, which is also known as the 'year without summer' (Stommel and Stommel 1979; Trigo et al. 2009) and occurs in reconstructions across the Northern Hemisphere as a cold year (Briffa et al. 1998; Frank et al. 2010) attributed to volcanic activity, particularly the massive Tambora eruption in 1815 (Wegmann et al. 2014). Other distinct negative peaks in the temperature reconstruction coincide with large tropical volcanic eruptions and extraordinarily cold years reported for the Northern Hemisphere (Fig. 5b). The 1641 eruption of the Parker volcano is the 3rd coldest year of the past 600 years in Briffa et al. (1998) and is also captured in the MXD series (−2.41 °C). Similarly, the 1835 Cosiguina, (−2.54 °C), 1884 Krakatau (−2.59 °C), and 1991 Pinatubo (−1.94 °C) eruptions are associated with cold summers reconstructed for Mt. Olympus. Other distinctive cold summers are not easily attributable to volcanism, but are consistent with more regional climatic extremes. Examples of such summers include 1699/1700 (−2.47 and −2.19 °C), for which Xoplaki et al. (2001) describes year-round snow cover over the Cretan mountains, poor harvest in Thessaly, and high animal mortality. The negative peak of 1959 (−3.27 °C) corresponds with an extremely cool summer throughout the Mediterranean (Xoplaki et al. 2003b) and is also anomalously cold in the Bulgarian temperature reconstruction developed by Trouet et al. (2012).

The climate response of Mt. Olympus PINI radial growth is consistent with other studies of this tree species (Lebourgeois 2000; Martín-Benito et al. 2008; Touchan et al. 2014). The LWW parameter contained a specific summer precipitation response with less carry-over effects prior to the growing season compared to TRW (Klesse 2012). Accordingly, we were able to skillfully reconstruct MJJ summer precipitation back to 1617. Several extreme summers reconstructed for Mt. Olympus broadly agree with other precipitation reconstructions of the eastern Mediterranean region. In their Standardized Precipitation Index (SPI) reconstruction for southern Turkey from *Juniperus excelsa* tree rings, Touchan et al. (2005) showed dry years from 1926 to 1929, with 1927 exceeding their drought threshold of −1.4. Purgstall (1983) reported a sustained famine in Anatolia from 1925 to 1928. In our study, these years are also characterized by low summer moisture values (in the context of the surrounding years with exceptional high values) with 1927 the driest year. More widespread anomalous conditions are supported by Akkemik and Aras (2005, PINI from Central Turkey). The sustained wet summers of 1691–1693 captured by our reconstruction (+1.71 sd) are reported as a pronounced period of unusually low sunshine in the western Balkans (Poljanšek et al. 2013). Similarly, the extremely dry summer of 1716 (−2.75 sd) was reported by Griggs et al. (2007) as exceptionally dry across the northern Aegean. Akkemik et al. (2008) describe 1715 and 1716 as a major dry event with a great famine reported for 1715 (Xoplaki et al. 2001). 1725 is one of the driest summers reconstructed for Mt. Olympus (−2.63 sd) and is also captured in reconstructions from Turkey (Akkemik and Aras 2005; Touchan et al. 2007) and Romania (Levanic et al. 2013). During the year 1780 heavy rainfall occurred in northern Greece (Xoplaki et al. 2001), which is also clearly recorded in our reconstruction in the context of the surrounding years with rather low values (+0.81 sd).

4.2 Reconstruction fidelity

The above comparisons suggest that many inter-annual to decadal precipitation and temperature extremes reconstructed for Mt. Olympus are spatially extensive across the northeastern Mediterranean and beyond. However, we are currently prohibited from comparing our low-frequency precipitation variability with other hydroclimatic reconstructions from across the Mediterranean because other studies have used methods that are only capable of retaining high-frequency climate variation. For example, Griggs et al. (2007) note in their title that their work is a "regional high-frequency reconstruction" as the tree-ring detrending and autoregressive modeling has removed all low frequency trends. Similar methods were applied in most, if not all, other northeastern Mediterranean tree-ring based reconstructions (e.g. Akkemik and Aras 2005; Touchan et al. 2005). In our study, we applied methods that are capable of retaining long-time scale climate variability from the tree-ring proxies. Our reconstructions show significant long-term deviations in hydroclimate over the past centuries with the nineteenth century notably dry and cool in comparison

to the twentieth century. Such long-term variations might not be expected based upon relatively short instrumental records, but are consistent with dramatic changes in hydroclimate across the globe during the past centuries (e.g., Stockton and Jacoby 1976). Right now there is no consensus for the spatial patterns or extremeness of twentieth century hydroclimatic conditions. Reconstructions from some regions suggest more pluvial conditions during much of the twentieth century [e.g. southeast Germany (Wilson et al. 2005), Pakistan (Treydte et al. 2006), the northeastern United States (Pederson et al. 2013)], while some show about average precipitation values [e.g. northern Europe (Helama et al. 2009), Central Europe (Büntgen et al. 2011, and Monsoon Asia (Cook et al. 2010)] and others dry [e.g. European Alps (Kress et al. 2014), Morocco (Esper et al. 2007), the southwestern United States (Cook et al. 2004)], or even wet spells [e.g. England (Wilson et al. 2013)] especially in the latest decades of the twentieth century. Our reconstruction provides new evidence that the Balkans experienced significant hydroclimatic variability during the past centuries and that the projected drying of up to 20 % (IPCC 2013) as well as the slight increase of summer precipitation (Hertig et al. 2013) would be in the range of past natural variability.

Nevertheless, caution is warranted when producing and interpreting reconstructions from tree rings with regard to the techniques applied to remove the biological age/size trend, the spectral characteristics in tree-ring time series, and the influence of other factors on tree growth in addition to the climate factor targeted for reconstruction. In order to investigate (and hopefully avoid) the possibility that detrending or sampling biases influence the long-term trends, we performed additional tests and found that the dramatic increase in the reconstructed precipitation around the turn of the twentieth century is also present if individual conservative detrending (e.g., negative exponential standardization) was applied (Fig. S2). Hence it can be dismissed that the twentieth century growth increase is related to a modern-sample bias (Briffa and Melvin 2011), as might be caused, for example, by the two young sites LIA and REB entering the regional chronology or the fact that no (XEP, PPP) or only few (PIGA) young trees (germination after 1850) contribute to the long higher elevation site chronologies. Prominent growth increases in the twentieth century are also evident in the raw TRW and LWW time series, further indicating that these reconstructed patterns are not an artifact of the applied detrending method.

Furthermore, similar trends and growth patterns observed for all investigated sites (Fig. 3a) suggest that if non-climatic disturbance contributed to the twentieth century growth increase, the disturbance was spatially extensive and occurred on all flanks of the Mt. Olympus massif, making it unlikely that windthrow from storms (Everham and Brokaw 1996) or fires reported for the late 19th century on the eastern side of Mt. Olympus (Habeck and Reif 1994) were responsible. Human management activities and animal grazing likely affected some of the forests, but are unlikely to result in such consistent disturbance patterns around the entire Mt. Olympus massif and are expected to have particularly modest, if any, effects on the particularly inaccessible sites located among rock/cliff faces. These rocky/cliff sites are also likely less susceptible to fires, windstorms, and other disturbance processes that are known to more strongly impact closed-canopy forests. Increasing the spatial coverage of precipitation sensitive time series across the northeastern Mediterranean will allow further testing of possible disturbances and more detailed assessments of the spatial patterns of hydroclimatic variability. New emphasis on datasets that are well-replicated and continued efforts to preserve long time-scale climate information should be prioritized. Identification and research at sites containing in situ relict material have particularly great potential to reduce uncertainties in benchmarking current climate conditions to pre-industrial variability.

It is broadly known that spectral properties of tree-ring time series are influenced by both climatic drivers and biological factors and can affect reconstruction fidelity. TRW tends to have a reddish spectrum, i.e., greater variance on longer rather than shorter time-scales, due to effects such as carbohydrate storage, leaf and root growth, and long-term disturbance effects (Fritts 1976; Meko 1981; Frank et al. 2007, 2013). The spectral characteristics of MXD are more poorly understood, but a recent analysis suggested that MXD time series tend to have whiter (i.e., more equal variance across all time-scales) spectra in comparison to TRW series and also possibly instrumental temperature data (Franke et al. 2013). By using LWW, which is less influenced by the previous year's climate and growth than TRW, we expected to obtain a greater fidelity to match the spectral domain of precipitation. Tests on the instrumental and reconstructed spectra (Fig. S3) suggest that the precipitation reconstruction spectrum does not differ substantially from the instrumental spectra during their common 1950–2010 period. Furthermore, the decadal to multi-decadal variability prior to the instrumental period is broadly centered around observed values during the recent decades. Similar results are found for the temperature reconstruction, but with a slight underestimation (overestimation) of the low (high) frequency variance. These results suggest that while some caution is warranted regarding the overall spectral characteristics of the reconstructions, they broadly support the overall shape and properties of hydroclimatic and temperature variability reconstructed for the past centuries.

4.3 Temperature and precipitation covariation

Similar to the instrumental observations, our temperature and precipitation reconstructions are negatively correlated with each other over the past four centuries both in the inter-annual to decadal and particularly the decadal to multi-decadal time-scales. This negative correlation serves to amplify possible drought effects through increased evaporative demand by high temperatures and contemporaneous reductions in rainfall, both expected for the future (Seneviratne et al. 2006). Current projections indicate a 2–3 °C increase in summer temperatures and up to 20 % decrease in summer precipitation for the Mediterranean region by 2100 (IPCC 2013). Land–atmosphere feedbacks are thought to modulate and amplify stress conditions associated with warm temperatures and soil moisture deficits (Seneviratne et al. 2006). Implications for both forest and agricultural activity include lower productivity and yields. Adaptation strategies may include the planting of more drought resistant crops and alternations in the planting and harvesting rhythms (Maracchi et al. 2005). Forest management strategies include promoting more heat/drought resistant cultivars or reducing transpiratory water losses through thinning of ecosystem (both over and understory) vegetation (Giuggiola et al. 2013).

Our reconstruction shows that the general co-variability between low precipitation and high temperatures apparent over the instrumental period does not necessarily hold on long time-scales. For example, in the 19th century there is no correlation between our temperature and precipitation reconstructions ($r = 0.0$), yet generally lower (late) summer temperatures coincide with overall drier (early) summer conditions. This is different to twentieth century temperature and precipitation co-variability. Similarly, Kress et al. (2014) reconstructed wet and warm conditions during Medieval times for the European Alps, whereas twentieth century warm temperatures were associated with dry conditions. The analysis of Central European climate data between 1780 and 1995 and the sea level pressure reconstruction from Luterbacher et al. (2002) revealed a majority of the summer climate variation in Europe could be attributed to internal changes of major atmospheric circulation patterns (Beck et al. 2007; Jacobeit et al. 2003). Such results suggest that changes in dynamical patterns can be superimposed upon shifts in long-term climatic baselines, and underscore the potential role of forced changes in both atmospheric dynamics and long-term temperature increase.

4.4 Spatiotemporal teleconnection dynamics

Spatial correlation analyses revealed a prominent dipole pattern across Europe that is consistent with the sNAO signature (Folland et al. 2009). The sNAO has previously been identified as the driving mode of summer air temperature variability in Greece on interannual as well as decadal scales (Xoplaki et al. 2003a) and as the main driver of drought events over the northeastern Mediterranean (Oikonomou et al. 2010). The prominent dipole has recently been reported in a summer temperature reconstruction for Bulgaria (Trouet et al. 2012) and in Hughes et al. (2001) in a network of drought sensitive chronologies from the eastern Mediterranean highlighting the importance of this circulation mode for tree growth in this region.

A July–August sNAO reconstruction (Linderholm et al. 2008, 2009) based on tree-ring data from northwestern Europe permitted the assessment of this dynamical mode back to 1441. The reconstruction is strongly correlated with twentieth century JJA precipitation over northern Europe (Pauling et al. 2006). However, the correlation declines dramatically parallel with the decrease of instrumental records in the early 1800s and generally low replication of precipitation sensitive proxy records in northern Europe in Pauling et al. (2006) before 1800. Surprisingly, Linderholm et al. (2009) found a weak negative relationship ($r = -0.16$, 1441–1995) with the eastern Mediterranean April–September PDSI reconstruction (averaged over 32.5–47.8 N, 10.8–30.8 E) by Brewer et al. (2006) instead of expected positive correlation inferred from the dipole pattern of the sNAO. In contrast to that, our MJJ precipitation reconstruction correlates positively over the full 1617–1995 period ($r = 0.21$, $p < 0.001$) with the sNAO reconstruction of Linderholm et al. (2009), with increasing r values ($r = 0.3$) when 15–100 year bandpass-filtering was applied. The slightly higher positive relationship during the twentieth century ($r = 0.23$, $p < 0.05$) and the particularly strong correlation of decadal to multidecadal variability ($r = 0.60$), coincides with an unprecedented pronounced negative correlation between the precipitation and temperature reconstructions from Mt. Olympus ($r = -0.65$).

The strongest previous evidence for a persistent teleconnection between summer climate conditions over the British Isles and the eastern Mediterranean was found in the Bulgarian summer temperature reconstruction (1768–2008) of Trouet et al. (2012). They suggested that the sNAO dipole signature is strong and stable over the period of overlap with the sNAO reconstruction of Folland et al. (2009, $r = -0.43$; $p < 0.001$, 1768–1976). Our temperature reconstruction yields similar, albeit slightly weaker correlations to the sNAO reconstruction of Folland et al. (2009) over the same period (1768–1976, $r = -0.25$; $p < 0.001$). Comparison of our temperature reconstruction with the Linderholm et al. (2009) sNAO reconstruction (1441–1995) allows testing the stability of this dipole even further back in time. Indeed, we find stable correlations between the sNAO and northeastern Mediterranean temperatures back to 1521 ($r = 0.33$; $p < 0.001$). Trouet et al. (2012) describe

a weakening in the correlation between Bulgarian tree-ring data and other records from the northern European dipole center including the sNAO index from 1795 to 1830. We also find weaker negative correlations in the late 1700s/early 1800s supporting hypotheses that this represents climatic dynamical phenomena (e.g., circulation responses to large volcanic eruptions) rather than reduced reconstruction quality as alternately discussed in Trouet et al. (2012). This again points to possible decoupling between the dominant atmospheric circulation patterns derived from twentieth century instrumental data and pre-industrial climate variability.

5 Conclusion

We present a multi parameter summer climate reconstruction for northern Greece extending back to 1617, which fills a gap, both in space and time, in the proxy evidence (Pauling et al. 2006; Luterbacher et al. 2004) for the southern node of the sNAO. The LWW chronology reflects MJJ precipitation and the MXD record relates strongly to JAS temperature. There is great consistency between warm and simultaneous dry decades in the twentieth century, but our reconstructions show that this co-variability does not necessarily hold on longer time-scales. The reconstructions indicate generally drier early summer conditions over the period 1700–1900 CE compared to the reference period (1950–2010) and simultaneously cooler late summer conditions, pointing towards a possible decoupling of the atmospheric circulation patterns derived from twentieth century instrumental data and pre-industrial climate variability. Further research on this topic should focus on a network analysis of well replicated datasets with long time-scale climate information and differing seasonal responses (e.g. MXD as late summer, TRW or LWW as early summer proxies) from both sides of the sNAO dipole to investigate the long-term behavior and dynamics of this important summer climate mode.

We show that summer temperatures of the last decade are at the upper end of reconstructed values, but not unprecedented. Recent summer precipitation values are comparable to similar conditions in the 2nd half of the seventeenth century. However, summer moisture limitations significantly lower than those observed in the late twentieth–early twenty-first century fall within the range of natural climate variability. This is particularly notable considering that current moisture availability already places severe limits on agricultural productivity, and thus both lends credibility to and caution for the significant drying trends projected for this region in current Earth System Model simulations. The projection of both warmer and drier summer climate poses challenges for human well-being, with increasing population requiring improved water management and the adaption of agricultural and silvicultural practices to counteract drought induced yield losses (García-Ruiz et al. 2011; Maracchi et al. 2005).

Acknowledgments The authors like to thank Patrick Fonti, Jörg Franke and Greg King for their help during fieldwork, and Anne Verstege for her help with the MXD measurements. We also thank Paul Krusic for discussion and helpful comments on the text and acknowledge financial support from the NSF CAREER Award AGS-1349942 (VT) and SNF iTREE sinergia project 136295 (SK, DF).

References

Akkemik Ü, Aras A (2005) Reconstruction (1689–1994 AD) of April–August precipitation in the southern part of central Turkey. Int J Climatol 25:537–548

Akkemik Ü, D'Arrigo R, Cherubini P et al (2008) Tree-ring reconstructions of precipitation and streamflow for north-western Turkey. Int J Climatol 28:173–183

Beck C, Jacobeit J, Jones PD (2007) Frequency and within-type variations of large-scale circulation types and their effects on low-frequency climate variability in central europe since 1780. Int J Climatol 27:473–491

Böhm R, Jones PD, Hiebl J et al (2010) The early instrumental warm-bias: a solution for long central European temperature series 1760–2007. Clim Change 101:41–67

Brewer S, Alleaume S, Guiot J, Nicault A (2006) Historical droughts in Mediterranean regions during the last 500 years: a data/model approach. Clim Past Discuss 2:771–800

Briffa KR, Melvin TM (2011) A closer look at regional curve standardization of tree-ring records: justification of the need, a warning of some pitfalls, and suggested improvements in its application. In: Hughes MK, Swetnam TW, Diaz HF (eds) Dendroclimatology. Springer, Netherlands, pp 113–145

Briffa KR, Jones PD, Schweingruber FH (1988) Summer temperature patterns over Europe: a reconstruction from 1750 A.D. based on maximum latewood density indices of conifers. Quat Res 30:36–52

Briffa KR, Jones PD, Bartholin TS et al (1992) Fennoscandian summers from ad 500: temperature changes on short and long timescales. Clim Dyn 7:111–119

Briffa KR, Jones PD, Schweingruber FH, Osborn TJ (1998) Influence of volcanic eruptions on Northern Hemisphere summer temperature over the past 600 years. Nature 393:450–455

Büntgen U, Frank DC, Nievergelt D, Esper J (2006) Summer temperature variations in the European Alps, a.d. 755–2004. J Clim 19:5606–5623

Büntgen U, Frank D, Grudd H, Esper J (2008) Long-term summer temperature variations in the Pyrenees. Clim Dyn 31:615–631

Büntgen U, Tegel W, Nicolussi K et al (2011) 2500 Years of European climate variability and human susceptibility. Science 331:578–582

Chronis T, Raitsos DE, Kassis D, Sarantopoulos A (2011) The Summer North Atlantic Oscillation influence on the Eastern Mediterranean. J Clim 24:5584–5596

Compo GP, Whitaker JS, Sardeshmukh PD et al (2011) The twentieth century reanalysis project. Quart J R Meteorol Soc 137:1–28

Cook ER, Kairiukstis LA (1990) Methods of dendrochronology: applications in the environmental sciences. Springer, New York

Cook ER, Briffa KR, Jones PD (1994) Spatial regression methods in dendroclimatology: a review and comparison of two techniques. Int J Climatol 14:379–402

Cook ER, Woodhouse CA, Eakin CM et al (2004) Long-term aridity changes in the Western United States. Science 306:1015–1018
Cook ER, Anchukaitis KJ, Buckley BM et al (2010) Asian Monsoon Failure and megadrought during the last millennium. Science 328:486–489
Dubrovský M, Hayes M, Duce P et al (2013) Multi-GCM projections of future drought and climate variability indicators for the Mediterranean region. Reg Environ Change. doi:10.1007/s10113-013-0562-z
Dünkeloh A, Jacobeit J (2003) Circulation dynamics of Mediterranean precipitation variability 1948–98. Int J Climatol 23:1843–1866
Eschbach W, Nogler P, Schär E, Schweingruber FH (1995) Technical advances in the radiodensitometrical determination of wood density. Dendrochronologia 13:155–168
Esper J, Frank DC, Wilson RJS, Briffa KR (2005) Effect of scaling and regression on reconstructed temperature amplitude for the past millennium. Geophys Res Lett 32:L07711
Esper J, Frank D, Büntgen U et al (2007) Long-term drought severity variations in Morocco. Geophys Res Lett 34:L17702. doi:10.1029/2007GL030844
Esper J, Düthorn E, Krusic PJ et al (2014) Northern European summer temperature variations over the Common Era from integrated tree-ring density records. J Quaternary Sci 29:487–494
Everham EM, Brokaw NVL (1996) Forest damage and recovery from catastrophic wind. Bot Rev 62:113–185
Fischer EM, Schär C (2010) Consistent geographical patterns of changes in high-impact European heatwaves. Nature Geosci 3:398–403
Folland CK, Knight J, Linderholm HW et al (2009) The summer North Atlantic oscillation: past, present, and future. J Clim 22:1082–1103
Frank D, Esper J (2005) Temperature reconstructions and comparisons with instrumental data from a tree-ring network for the European Alps. Int J Climatol 25:1437–1454
Frank D, Esper J, Cook ER (2006) On variance adjustments in tree-ring chronology development. Tree Ring Archaeol Clim Ecol 4:56–66
Frank D, Büntgen U, Böhm R et al (2007) Warmer early instrumental measurements versus colder reconstructed temperatures: shooting at a moving target. Quat Sci Rev 26:3298–3310
Frank DC, Esper J, Raible CC et al (2010) Ensemble reconstruction constraints on the global carbon cycle sensitivity to climate. Nature 463:527–530
Franke J, Frank D, Raible CC et al (2013) Spectral biases in tree-ring climate proxies. Nature Clim Change 3:360–364
Fritts HC (1976) Tree rings and climate. London
Gao X, Giorgi F (2008) Increased aridity in the Mediterranean region under greenhouse gas forcing estimated from high resolution simulations with a regional climate model. Global Planet Change 62:195–209
García-Ruiz JM, López-Moreno JI, Vicente-Serrano SM et al (2011) Mediterranean water resources in a global change scenario. Earth Sci Rev 105:121–139
Giorgi F, Lionello P (2008) Climate change projections for the Mediterranean region. Global Planet Change 63:90–104
Giuggiola A, Bugmann H, Zingg A et al (2013) Reduction of stand density increases drought resistance in xeric Scots pine forests. For Ecol Manage 310:827–835
Griffin D, Meko DM, Touchan R et al (2011) Latewood chronology development for summer-moisture reconstruction in the US Southwest. Tree-Ring Research 67:87–101
Griggs C, DeGaetano A, Kuniholm P, Newton M (2007) A regional high-frequency reconstruction of May–June precipitation in the north Aegean from oak tree rings, A.D. 1089–1989. Int J Climatol 27:1075–1089
Grudd H (2008) Torneträsk tree-ring width and density ad 500–2004: a test of climatic sensitivity and a new 1500-year reconstruction of north Fennoscandian summers. Clim Dyn 31:843–857
Habeck F, Reif A (1994) Die Waldgesellschaften der montanen und subalpinen Stufe des Ostabfalls des Olymp, Griechenland. Phytocoenologia 22:501–536
Haylock MR, Hofstra N, Klein Tank AMG et al (2008) A European daily high-resolution gridded data set of surface temperature and precipitation for 1950–2006. J Geophys Res 113:D20119
Helama S, Meriläinen J, Tuomenvirta H (2009) Multicentennial megadrought in northern Europe coincided with a global El Niño-Southern Oscillation drought pattern during the Medieval Climate Anomaly. Geology 37:175–178
Hertig E, Jacobeit J (2008) Assessments of Mediterranean precipitation changes for the 21st century using statistical downscaling techniques. Int J Climatol 28:1025–1045
Hertig E, Seubert S, Paxian A et al (2013) Changes of total versus extreme precipitation and dry periods until the end of the twenty-first century: statistical assessments for the Mediterranean area. Theor Appl Climatol 111:1–20
Holmes RL (1983) Computer-assisted quality control in tree-ring dating and measurement. Tree Ring Bull 43:69–78
Hughes MK, Kuniholm PI, Eischeid JK et al (2001) Aegean tree-ring signature years explained. Tree Ring Res 57:67–73
IPCC (2013) Climate change 2013: the physical science basis. In: Stocker TF, Qin D, Plattner G-K, Tignor M, Allen SK, Boschung J, Nauels A, Xia Y, Bex V, Midgley PM (eds) Contribution of working group i to the fifth assessment report of the intergovernmental panel on climate change. Cambridge University Press, Cambridge, 1535 pp
Jacobeit J, Wanner H, Luterbacher J et al (2003) Atmospheric circulation variability in the North-Atlantic-European area since the mid-seventeenth century. Clim Dyn 20:341–350
Klein Tank AMG, Wijngaard JB, Können GP et al (2002) Daily dataset of 20th-century surface air temperature and precipitation series for the European climate assessment. Int J Climatol 22:1441–1453
Klesse S (2012) Response of Pinus nigra to long-term moisture variability on Mt. Olympus, Greece. Diploma thesis. Mainz
Klesse S, Frank D (2013) The application of regional curve standardization on living tree datasets. Tree Ring Archaeol Clim Ecol 11:47–55
Köse N, Akkemik Ü, Dalfes HN, Özeren MS (2011) Tree-ring reconstructions of May–June precipitation for western Anatolia. Quat Res 75:438–450
Kress A, Hangartner S, Bugmann H et al. (2014) Swiss tree rings reveal warm and wet summers during medieval times. Geophys Res Lett 41:2013GL059081. doi:10.1002/2013GL059081
Krichak SO, Alpert P (2005) Decadal trends in the east Atlantic–west Russia pattern and Mediterranean precipitation. Int J Climatol 25:183–192
Lebourgeois F (2000) Climatic signals in earlywood, latewood and total ring width of Corsican pine from western France. Ann For Sci 57:55–164
Lenz O, Schär E, Schweingruber FH (1976) Methodische Probleme bei der radiographisch-densitometrischen Bestimmung der Dichte und der Jahrringbreiten von Holz. Holzforschung 30:114–123
Levanič T, Popa I, Poljanšek S, Nechita C (2013) A 323-year long reconstruction of drought for SW Romania based on black pine (Pinus Nigra) tree-ring widths. Int J Biometeorol 57:703–714
Linderholm HW, Folland CK, Hurrell JW (2008) Reconstructing Summer North Atlantic Oscillation (SNAO) variability over the last five centuries. Tree Ring Archaeol Clim Ecol 6:8–16
Linderholm HW, Folland CK, Walther A (2009) A multicentury perspective on the summer North Atlantic Oscillation (SNAO) and drought in the eastern Atlantic Region. J Quat Sci 24:415–425
Lindner M, Maroschek M, Netherer S et al (2010) Climate change impacts, adaptive capacity, and vulnerability of European forest ecosystems. For Ecol Manage 259:698–709

Luterbacher J, Xoplaki E, Dietrich D et al (2002) Reconstruction of sea level pressure fields over the Eastern North Atlantic and Europe back to 1500. Clim Dyn 18:545–561

Luterbacher J, Dietrich D, Xoplaki E et al (2004) European seasonal and annual temperature variability, trends, and extremes since 1500. Science 303:1499–1503

Luterbacher J, Koenig SJ, Franke J et al (2010) Circulation dynamics and its influence on European and Mediterranean January–April climate over the past half millennium: results and insights from instrumental data, documentary evidence and coupled climate models. Clim Change 101:201–234

Maracchi G, Sirotenko O, Bindi M (2005) Impacts of present and future climate variability on agriculture and forestry in the temperate regions: Europe. Clim Change 70:117–135

Mariotti A, Arkin P (2007) The North Atlantic oscillation and oceanic precipitation variability. Clim Dyn 28:35–51

Mariotti A, Dell'Aquila A (2012) Decadal climate variability in the Mediterranean region: roles of large-scale forcings and regional processes. Clim Dyn 38:1129–1145

Martín-Benito D, Cherubini P, del Río M, Cañellas I (2008) Growth response to climate and drought in Pinus nigra Arn. trees of different crown classes. Trees 22:363–373

Meko DM (1981) Applications of Box-Jenkins methods of time series analysis to the reconstruction of drought from tree rings. Dissertation. Tucson

Meko DM, Baisan CH (2001) Pilot study of latewood-width of conifers as an indicator of variability of summer rainfall in the North American monsoon region. Int J Climatol 21:697–708

Melvin TM, Briffa KR (2008) A "signal-free" approach to dendroclimatic standardisation. Dendrochronologia 26:71–86

Melvin TM, Briffa KR, Nicolussi K, Grabner M (2007) Time-varying-response smoothing. Dendrochronologia 25:65–69

Mitchell TD, Jones PD (2005) An improved method of constructing a database of monthly climate observations and associated high-resolution grids. Int J Climatol 25:693–712. doi:10.1002/joc.1181

Moriondo M, Good P, Durao R et al (2006) Potential impact of climate change on fire risk in the Mediterranean area. Clim Res 31:85–95

NCDC (2011) National Climate Data Center (2011) The International Tree Ring Data Bank. http://www.ncdc.noaa.gov/paleo/treering.html. 21 May 2014

Nicault A, Alleaume S, Brewer S et al (2008) Mediterranean drought fluctuation during the last 500 years based on tree-ring data. Clim Dyn 31:227–245

Oikonomou C, Flocas HA, Hatzaki M et al (2010) Relationship of extreme dry spells in Eastern Mediterranean with large-scale circulation. Theor Appl Climatol 100:137–151

Önol B, Semazzi FHM (2009) Regionalization of climate change simulations over the Eastern Mediterranean. J Clim 22:1944–1961

Önol B, Bozkurt D, Turuncoglu UU et al (2014) Evaluation of the twenty-first century RCM simulations driven by multiple GCMs over the Eastern Mediterranean-Black Sea region. Clim Dyn 42:1949–1965

Pauling A, Luterbacher J, Casty C, Wanner H (2006) Five hundred years of gridded high-resolution precipitation reconstructions over Europe and the connection to large-scale circulation. Clim Dyn 26:387–405

Pederson N, Bell AR, Cook ER et al (2013) Is an epic pluvial masking the water insecurity of the greater New York city region. J Clim 26:1339–1354

Planton S, Lionello P, Artale V et al (2012) The climate of the Mediterranean region in future climate projections. The Climate of the Mediterranean Region. Elsevier, Amsterdam, pp 449–502

Poljanšek S, Baillan D, Nage T, Levanic T (2012) A 435-year-long European black pine (*Pinus nigra*) chronology for the central-western Balkan region. Tree Ring Res 68:1–44

Poljanšek S, Ceglar A, Levanič T (2013) Long-term summer sunshine/moisture stress reconstruction from tree-ring widths from Bosnia and Herzegovina. Clim Past 9:27–40

Popa I, Bouriaud O (2014) Reconstruction of summer temperatures in Eastern Carpathian Mountains (Rodna Mts, Romania) back to AD 1460 from tree-rings. Int J Climatol 34:871–880

Purgstall B (1983) Ottoman state history, vol 1–7. Istanbul

Quadrelli R, Pavan V, Molteni F (2001) Wintertime variability of Mediterranean precipitation and its links with large-scale circulation anomalies. Clim Dyn 17:457–466

Rinn F (2003) Time series analysis and presentation for dendrochronology and related applications. Heidelberg

Schröter D, Cramer W, Leemans R et al (2005) Ecosystem service supply and vulnerability to global change in Europe. Science 310:1333–1337

Schweingruber FH (1989) Tree rings: basics and applications of dendrochronology. Dordrecht

Seim A, Büntgen U, Fonti P et al (2012) Climate sensitivity of a millennium-long pine chronology from Albania. Clim Res 51:217–228

Seneviratne SI, Lüthi D, Litschi M, Schär C (2006) Land–atmosphere coupling and climate change in Europe. Nature 443:205–209

Stockton CW, Jacoby GCJ (1976). Long-term surfacewater supply and streamflow trends in the Upper Colorado River Basin based on tree-ring analysis. Lake Powell Res Project Bull 18:70

Stokes MA, Smiley T (1968) An introduction to tree-ring dating. University of Chicago Press, Chicago

Stommel H, Stommel E (1979) Volcano weather: the story of 1816, the year without summer. Seven Seas Press, Newport

Strid A (1980) Wild flowers of Mount Olympus. Athens

Thompson DWJ, Kennedy JJ, Wallace JM, Jones PD (2008) A large discontinuity in the mid-twentieth century in observed global-mean surface temperature. Nature 453:646–649

Touchan R, Garfin GM, Meko DM et al (2003) Preliminary reconstructions of spring precipitation in southwestern Turkey from tree-ring width. Int J Climatol 23:157–171

Touchan R, Xoplaki E, Funkhouser G et al (2005) Reconstructions of spring/summer precipitation for the Eastern Mediterranean from tree-ring widths and its connection to large-scale atmospheric circulation. Clim Dyn 25:75–98

Touchan R, Akkemik Ü, Hughes MK, Erkan N (2007) May–June precipitation reconstruction of southwestern Anatolia, Turkey during the last 900 years from tree rings. Quat Res 68:196–202

Touchan R, Anchukaitis KJ, Shishov VV et al (2014) Spatial patterns of eastern Mediterranean climate influence on tree growth. Holocene 24:381–392

Trachsel M, Kamenik C, Grosjean M et al (2012) Multi-archive summer temperature reconstruction for the European Alps, AD 1053–1996. Quat Sci Rev 46:66–79

Treydte KS, Schleser GH, Helle G et al (2006) The twentieth century was the wettest period in northern Pakistan over the past millennium. Nature 440:1179–1182

Trigo RM, Osborn TJ, Corte-Real JM (2002) The North Atlantic Oscillation influence on Europe: climate impacts and associated physical mechanisms. Clim Res 20:9–17

Trigo RM, Vaquero JM, Alcoforado M-J et al (2009) Iberia in 1816, the year without a summer. Int J Climatol 29:99–115

Trouet V (in press) A tree-ring based late summer temperature reconstruction (1675–1980) for the northeastern Mediterranean. Tree-Ring Res

Trouet V, Van Oldenborgh GJ (2013) KNMI climate explorer: a web-based research tool for high-resolution paleoclimatology. Tree Ring Res 69:3–13

Trouet V, Panayotov MP, Ivanova A, Frank D (2012) A pan-European summer teleconnection mode recorded by a new temperature reconstruction from the northeastern Mediterranean (ad 1768–2008). Holocene 22:887–898

Van Oldenborgh GJ, Burgers G (2005) Searching for decadal variations in ENSO precipitation teleconnections. Geophys Res Lett 32:L15701

Wegmann M, Brönnimann S, Bhend J et al (2014) Volcanic influence on European Summer precipitation through monsoons: possible cause for "Years without Summer". J Clim 27:3683–3691

Wigley TML, Briffa KR, Jones PD (1984) On the average value of correlated time series with applications in dendroclimatology and hydrometeorology. J Clim Appl Meteorol 23:201–213

Wilson RJS, Luckman BH, Esper J (2005) A 500 year dendroclimatic reconstruction of spring–summer precipitation from the lower Bavarian Forest region, Germany. Int J Climatol 25:611–630

Wilson R, Miles D, Loader NJ et al (2013) A millennial long March–July precipitation reconstruction for southern-central England. Clim Dyn 40:997–1017

Xoplaki E, Maheras P, Luterbacher J (2001) Variability of climate in Meridional Balkans during the Periods 1675–1715 and 1780–1830 and its impact on human life. Clim Change 48:581–615

Xoplaki E, González-Rouco J, Gyalistras D et al (2003a) Interannual summer air temperature variability over Greece and its connection to the large-scale atmospheric circulation and Mediterranean SSTs 1950–1999. Clim Dyn 20:537–554

Xoplaki E, González-Rouco JF, Luterbacher J, Wanner H (2003b) Mediterranean summer air temperature variability and its connection to the large-scale atmospheric circulation and SSTs. Clim Dyn 20:723–739

Xoplaki E, González-Rouco JF, Luterbacher J, Wanner H (2004) Wet season Mediterranean precipitation variability: influence of large-scale dynamics and trends. Clim Dyn 23:63–78

Zumbühl HJ, Steiner D, Nussbaumer SU (2008) 19th century glacier representations and fluctuations in the central and western European Alps: an interdisciplinary approach. Global Planet Change 60:42–57